



## Article

# Construction of TiO<sub>2</sub>-Eggshell for Efficient Degradation of Tetracycline Hydrochloride: Sunlight Induced In-Situ Formation of Carbonate Radical

Zhuquan Huang <sup>1,2</sup>, Jiaqi Wang <sup>1,2</sup>, Min-Quan Yang <sup>1,2</sup>, Qingrong Qian <sup>1,2</sup>, Xin-Ping Liu <sup>1,2</sup>, Liren Xiao <sup>1,2,\*</sup> and Hun Xue <sup>1,2,\*</sup>

<sup>1</sup> College of Environmental Science and Engineering, Fujian Normal University, Fuzhou 350007, China; ZhuquanHuang0530@163.com (Z.H.); jiaqiwang77@126.com (J.W.); yangmq@fjnu.edu.cn (M.-Q.Y.); qrqian@fjnu.edu.cn (Q.Q.); lxpwkm@fjnu.edu.cn (X.-P.L.)

<sup>2</sup> Fujian Key Laboratory of Pollution Control & Resource Reuse, Fujian Normal University, Fuzhou 350007, China

\* Correspondence: xlr1966@fjnu.edu.cn (L.X.); xuehun@fjnu.edu.cn (H.X.)

**Abstract:** Photocatalytic degradation of an antibiotic by utilizing inexhaustible solar energy represents an ideal solution for tackling global environment issues. The target generation of active oxidative species is highly desirable for the photocatalytic pollutants degradation. Herein, aiming at the molecular structure of tetracycline hydrochloride (TC), we construct sunlight-activated high-efficient catalysts of TiO<sub>2</sub>-eggshell (TE). The composite ingeniously utilizes the photoactive function of TiO<sub>2</sub> and the composition of eggshell, which can produce oxidative ·CO<sub>3</sub><sup>−</sup> species that are especially active for the degradation of aromatic compounds containing phenol or aniline structures. Through the synergistic oxidation of the ·CO<sub>3</sub><sup>−</sup> with the traditional holes (h<sup>+</sup>), superoxide radicals (·O<sub>2</sub><sup>−</sup>) and hydroxyl radicals (·OH) involved in the photocatalytic process, the optimal TE photocatalyst degrades 92.0% TC in 30 min under solar light, which is higher than TiO<sub>2</sub> and eggshell. The photocatalytic degradation pathway of TC over TE has been proposed. The response surface methodology is processed by varying four independent parameters (TC concentration, pH, catalyst dosage and reaction time) on a Box–Behnken design (BBD) to optimize the experimental conditions. It is anticipated that the present work can facilitate the development of novel photocatalysts for selective oxidation based on ·CO<sub>3</sub><sup>−</sup>.

**Keywords:** photocatalysis; TiO<sub>2</sub>-eggshell; carbonate radical; tetracycline hydrochloride; selective oxidation



**Citation:** Huang, Z.; Wang, J.; Yang, M.-Q.; Qian, Q.; Liu, X.-P.; Xiao, L.; Xue, H. Construction of TiO<sub>2</sub>-Eggshell for Efficient Degradation of Tetracycline Hydrochloride: Sunlight Induced In-Situ Formation of Carbonate Radical. *Materials* **2021**, *14*, 1598. <https://doi.org/10.3390/ma14071598>

Academic Editor: Dror Avisar

Received: 4 February 2021

Accepted: 12 March 2021

Published: 25 March 2021

**Publisher's Note:** MDPI stays neutral with regard to jurisdictional claims in published maps and institutional affiliations.



**Copyright:** © 2021 by the authors. Licensee MDPI, Basel, Switzerland. This article is an open access article distributed under the terms and conditions of the Creative Commons Attribution (CC BY) license (<https://creativecommons.org/licenses/by/4.0/>).

## 1. Introduction

In recent years, the antibiotics residuals in the water environment increase gradually, which has become a serious problem for policy-makers, scientists and the public [1–4]. Tetracycline hydrochloride (TC) is one of the ten antimicrobials licensed for the promotion of livestock growth, which is now detected in significant amounts in potable, sewage water and sediment [5]. Moreover, due to its biorefractory and stable nature, the increased presence of TC in aquatic environments has raised great concerns for both environment and human health [6,7]. Therefore, developing efficient technology to eliminate TC from an aqueous environment is urgently required.

Photocatalysis is a promising strategy for environmental remediation, because it can utilize solar light directly, react at ambient temperature and has no secondary pollution [8]. The application of photocatalysis technology in the degradation of TC has been carried out. It has been found that photocatalysts such as TiO<sub>2</sub>, WO<sub>3</sub> and C<sub>3</sub>N<sub>4</sub> have the performance of photocatalytic degradation of TC [9–12]. At present, however, the active oxygen species involved in these photocatalytic systems are mainly hydroxyl radicals (·OH) and superoxide radicals (·O<sub>2</sub><sup>−</sup>), which are impossible to specifically degrade TC according to its molecular

structure, resulting in insufficient degradation efficiency, incomplete degradation and easy inactivation of photocatalysts [13–15]. Therefore, the key point towards the application of photocatalysis in the degradation of TC is, targeting to molecular structure of TC and utilizing a new degradation mechanism, to develop highly efficient sunlight responsive photocatalysts.

Carbonate radical ( $\cdot\text{CO}_3^-$ ) is a powerful one-electron oxidant, which displays high selectivity for the degradation of aromatic compounds containing phenol or aniline structures [16,17]. It has been observed that adding a certain concentration of  $\text{CO}_3^{2-}$  in solution can significantly enhance the photocatalytic degradation rate of organic pollutants, such as oxytetracycline and aniline, which can be ascribed to the reaction between  $\cdot\text{OH}$  or holes ( $h^+$ ) produced from the photocatalysis process and  $\text{HCO}_3^-$  or  $\text{CO}_3^{2-}$  to generate  $\cdot\text{CO}_3^-$  [18–21].

It is known to us that TC is an aromatic compound that contains the structure of phenol in detail. According to the characteristics of selective oxidation of  $\cdot\text{CO}_3^-$ , the introduction of  $\cdot\text{CO}_3^-$  in the photocatalytic system is expected to enhance the degradation efficiency of TC. However, adding a certain amount of  $\text{CO}_3^{2-}$  to the solution not only increases the treatment cost, but also introduces new pollutants, which may cause side reactions in the photocatalytic process. Additionally, the formation of  $\cdot\text{CO}_3^-$  is affected by the movement rate of  $\text{CO}_3^{2-}$ , the migration and transformation of photoinduced carries and reactive oxygen species (ROS) at the solid-liquid interface [19]. Therefore, if  $\cdot\text{CO}_3^-$  can be generated in-situ on the surface of the photocatalyst, it can overcome the loss of photogenerated carriers and ROS due to its transfer and transformation at the solid-liquid interface and then improve the generation rate and yield of  $\cdot\text{CO}_3^-$ , which can greatly improve the selective oxidation ability of the photocatalyst.

$\text{TiO}_2$  has been the most widely used photocatalyst due to its non-toxic, chemically stable and appropriate UV-light response range [22]. Based on the characteristics of surface hydroxylation of  $\text{CaCO}_3$  in the aqueous system,  $\text{TiO}_2\text{-CaCO}_3$  can be constructed through the surface hydroxyl group at the phase interface of  $\text{CaCO}_3$  and  $\text{TiO}_2$ . Then  $\cdot\text{CO}_3^-$  is expected to generate in-situ on the catalyst surface [23]. Recently we reported  $\text{TiO}_2$ -seashell composites (seashell contain more than 95%  $\text{CaCO}_3$ ) exhibited excellent solar light-driven photochemical activity in the decomposition of tetracycline hydrochloride, due to the role of  $\cdot\text{CO}_3^-$  in promoting the degradation process [24].

As a significant byproduct of poultry eggs, eggshells contain 94–97 wt.%  $\text{CaCO}_3$ , which are eco-friendliness, low cost, nontoxicity and easy to collect [25]. It can be used as a carrier for nanomaterials due to the randomized porous structure [26]. Preparing  $\text{TiO}_2$ -eggshells composites cannot only generate  $\cdot\text{CO}_3^-$  species for TC elimination under light illumination but also obtain the photocatalysts with a porous structure.

In the present work, the  $\text{TiO}_2$ -eggshell composite was synthesized by a sol-gel method and used as a photocatalyst for the degradation of TC under solar light irradiation. The possible degradation pathway is proposed and the photocatalytic mechanism of TC degradation over  $\text{TiO}_2$ -eggshell is validated. Response surface methodology (RSM) is applied to optimize the reaction conditions and further evaluate the interaction among the selected process parameters. This work is expected to provide a novel and practical reference for the design and preparation of selective oxidation photocatalytic materials based on in situ generation of  $\cdot\text{CO}_3^-$ .

## 2. Methods and Materials

### 2.1. Chemical and Reagents

Titanium tetraisopropoxide ( $\text{C}_{12}\text{H}_{28}\text{O}_4\text{Ti}$ , 97%) was purchased from Sigma-Aldrich (Shanghai, China). Tetracycline hydrochloride (TC, 96%), 4-chlorophenol (4-CP, 99%), ammonium oxalate (AO, 99.8%), benzoquinone (BQ, 99%) and isopropyl alcohol (IPA,  $\geq 99.5\%$ ) were provided by Aladdin (Shanghai, China). Waste eggshells were collected from a restaurant in Fuzhou, China. All chemicals were of analytical grade and used as received without further purification.

## 2.2. Synthesis Process

Eggshells with the films removed were obtained from raw chicken eggs and washed. Briefly, the collected eggshells were washed with distilled water, oven dried overnight at 80 °C for constant mass. The eggshell was calcined at 300 °C for 5 h, then the obtained powder was milled, sieved to a particle size below ca. 150 µm. The received powder was remarked as eggshell.

Sol-gel method was applied to synthesize TiO<sub>2</sub>. Firstly, titanium tetraisopropoxide was hydrolyzed in acidic conditions and further dialyzed to pH=4. In a typical combustion method, pure TiO<sub>2</sub> powder was obtained through the calcination of transparent TiO<sub>2</sub> sol under 300 °C for 5 h [27]. Of TiO<sub>2</sub> 3.0 g was obtained by calcining 100 mL of TiO<sub>2</sub> sol. The white powder was marked as TiO<sub>2</sub>.

To obtain the TiO<sub>2</sub>-eggshell composite, 1.8 g of eggshell was dispersed in 40 mL of TiO<sub>2</sub> sol and stirred for 2 h at ambient temperature. After being dehydrated in a microwave oven, the gels were calcined in a muffle furnace at 5 °C/min to a fixed temperature of 300 °C and maintained for 5 h. Subsequently, the obtained powders were labeled as TE.

## 2.3. Characterization and Analytical Methods

Surface morphology of all samples was obtained by scanning electron microscopy (SEM) recorded on a Regulus 8100 field emission (Tokyo, Japan) and high resolution transmission electron microscopy (HRTEM Tecnai G2 F20, Boerne, TX, USA) at 200 kV accelerating voltage. Crystal structures of the as-synthesized samples were identified through an X-ray diffractometer (XRD) using filtered Cu-K $\alpha$  radiation and scanned in the range of 10–80° at 40 kV. F(R) were measured by a CARY-100 spectrophotometer (Agilent), in which BaSO<sub>4</sub> powder was used as an internal standard to obtain the optical properties of the samples over a wavelength range of 200–800 nm. The Brunauer–Emmett–Teller (BET, Osaka, Japan) specific surface area and nitrogen adsorption-desorption isotherms were carried out on a BELSORP-mini II nitrogen adsorption-desorption apparatus. Samples were pretreated at 120 °C for 2 h in vacuum to remove moisture and other gases before the test. Fourier infrared spectroscopy (FT-IR, Waltham, MA, USA) was measured in a frequency range of 4000–400 cm<sup>-1</sup> on a Thermo Scientific Nicolet spectrometer. In this part, the resultant suspension was filtered through a porous membrane (0.45 µm) and the filtrate was analyzed after freeze-drying (KBr is used to press platelets).

The degradation products of TC were detected and identified by a liquid chromatography-quadrupole time-of-flight tandem mass spectrometry (LC-QTOF-MS, Malvern, UK) system equipped with an Agilent Zorbax SB-C18 (4.6 mm × 150 mm, 5 µm). Mobile phase A was aqueous formic acid solution (0.1%, *v/v*), and mobile phase B was acetonitrile. The gradient solvent was at a flow rate of 1 mL/min as follows: A = 90% (0 min), 75% (3 min), 65% (6 min), 60% (9 min) and 60% (12 min). The injection volume was 8 µL and the column temperature was maintained at 25 °C. The MS was performed in a positive electrospray ion mode (ESI+) under the followed conditions: fragmentor 140 V, cone voltage 65 V and nitrogen gas flow rate 10 L/min with a temperature of 350 °C. MS was full scanned by mass and this ranged from 200 to 550 *m/z*.

## 2.4. Photochemical Measurements

Photochemical activities of the TiO<sub>2</sub>-eggshell composite were evaluated by monitoring the photodegradation of tetracycline hydrochloride (TC). A 300 W Xenon lamp (PLS-SXE300, Beijing Perfect Light Co.; Beijing, China) was employed as the light source equipped with an AM 1.5 simulated solar filter (200–1200 nm). In a typical procedure, 100 mg of the as-prepared sample was dispersed in 100 mL of 50 mg/L TC aqueous solution in a glass vessel with reflux water at ambient temperature. Before irradiation, the mixed suspension was constantly stirred for 3 h in the dark to obtain absorption-desorption equilibrium. The concentration of TC at absorption-desorption equilibrium was defined as the initial concentration C<sub>0</sub>. Subsequently, the suspension was illuminated and 4 mL solution was sampled after being centrifuged immediately to remove the powder at 5 min

intervals. Then the concentration of TC in the resulting clear solution was analyzed by a Shimadzu UV–vis spectrophotometer (UV-1750, San Diego, CA, USA) at a detection wavelength of 357 nm [15]. The degradation efficiency was described as Equation (1):

$$E\% = 1 - (C/C_0) \% \quad (1)$$

### 2.5. Tetracycline Hydrochloride (TC) Degradation Using Response Surface Methodology

Response surface methodology experiments were developed to optimize the reaction conditions via the Design Expert delicate product (version, 8.0.6) based on the Box–Behnken design (BBD). The total experiment set comprised four factors, pH (A), concentration (B), dosage (C) and temperature (D), each at three levels (−1, 0, 1) (Table 1). A quadratic polynomial model was applied to the response surface in terms of the four independent variables and described as Equation (2) [28,29].

$$Y = b_0 + \sum_{i=1}^n b_i x_i + \sum_{i=1}^n b_{ii} x_i^2 + \sum_{i \neq j}^n b_{ij} x_i x_j + \varepsilon \quad (2)$$

where Y is the predicted TC degradation efficiency,  $b_0$ ,  $b_i$ ,  $b_{ii}$  and  $b_{ij}$  are equal to regression constants, which represent the model, linear, quadratic and interaction coefficient, respectively.  $x_i$  and  $x_j$  are the independent variables in coded values, n means the number of independent variables and  $\varepsilon$  is described as the model error. In addition, the analysis of variance (ANOVA) is applied to assess the validity of the regression model, while the fit quality of the model is judged by the correlation coefficient ( $R^2$ ) and F test confirms the statistical significance.

**Table 1.** Independent variables and levels used for response surface methodology (RSM).

Factors	Levels		
	Low (−1)	Medium (0)	High (+1)
A: Irradiation time (min)	2	16	30
B: Dosage ( $\text{g}\cdot\text{L}^{-1}$ )	0.02	0.1	0.18
C: pH	6	8.5	11
D: Concentration ( $\text{mg}\cdot\text{L}^{-1}$ )	20	50	80

### 3. Results and Discussion

The crystal structure of  $\text{TiO}_2$ , eggshell and TE was characterized by XRD and the results are exhibited in Figure 1. The diffraction peaks of  $\text{TiO}_2$  can be indexed to anatase  $\text{TiO}_2$  (JCPDS No. 21-1272). The correlative diffraction peaks at 25.3, 37.8, 48.1, 53.9 and 55.1° correspond to (101), (004), (200), (105) and (211) crystal planes, respectively [30]. All diffraction peaks of pure eggshell matched well with  $\text{CaCO}_3$  in the form of calcite, which is consistent with the previous study [31]. TE presents both the characteristic diffraction peaks of anatase  $\text{TiO}_2$  and  $\text{CaCO}_3$ , demonstrating the coexistence of the two components. The result also verifies that  $\text{TiO}_2$  has no obvious influence on the crystal structure of eggshell. Additionally, the average crystal diameters of  $\text{TiO}_2$  in the samples have been calculated from the Scherrer equation based on the half-width of the (101) peak of anatase  $\text{TiO}_2$ , which reveal that the average diameters are both around 6 nm.

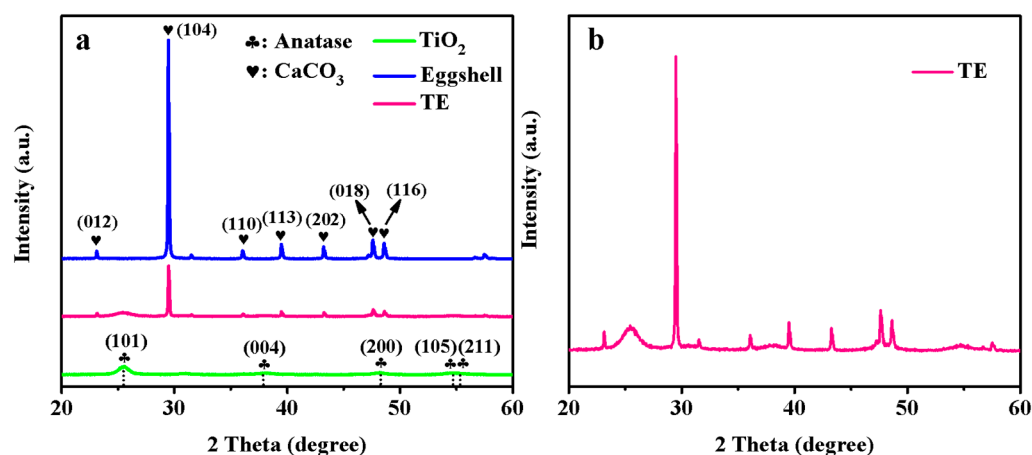


**Figure 1.** X-ray diffractometer (XRD) pattern of (a) the as-synthesized samples and (b) TiO<sub>2</sub>-eggshell composite (TE) in detail.

To examine the light absorption of pure TiO<sub>2</sub>, eggshell and TE composite, UV-visible diffuse reflectance spectra analysis has been carried out and the result is shown in Figure 2. For pure TiO<sub>2</sub>, the absorption band edge was found at *ca.* 410 nm, corresponding to an intrinsic band gap of 3.02 eV. In contrast, the pure eggshell displays weak absorption in the UV-visible region without obvious absorption edge. In addition, after the hybridization of TiO<sub>2</sub> with eggshell, the absorption band edge of TE is observed at 400 nm.

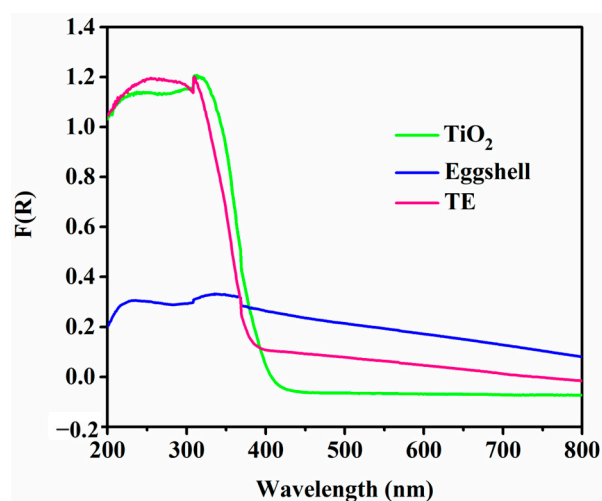


**Figure 2.** UV-visible diffuse reflectance spectra of TiO<sub>2</sub>, eggshell and TE.

Nitrogen physisorption measurement is applied to investigate the structure properties of TiO<sub>2</sub>, eggshell and TE. As shown in Figure 3, the adsorption–desorption isotherms (Figure 3a) of TiO<sub>2</sub> and TE both display a type IV feature with a well-defined hysteresis loop, which is an indication of well-developed mesoporous materials. As confirmed by the Barrett-Joyner-Halenda (BJH) pore size distribution analysis, the average pore diameters (Figure 3b) were about 7.5, 34.6 and 7.5 nm for TiO<sub>2</sub>, eggshell and TE, respectively. As for eggshell, it shows a type II feature. The BET surface areas of TiO<sub>2</sub>, eggshell and TE were estimated to be 125.4, 1.8 and 91.7 m<sup>2</sup>·g<sup>−1</sup>, respectively.



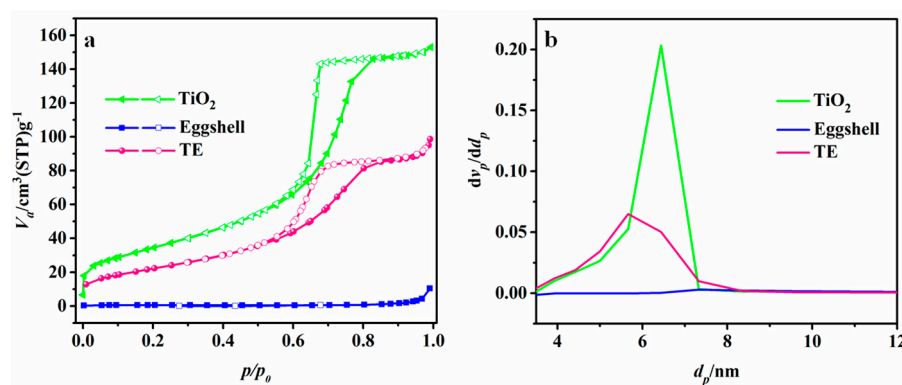


**Figure 3.** (a)  $N_2$  adsorption–desorption isotherms and (b) pore size distribution of the as-obtained samples.

The SEM images of the samples are shown in Figure 4. It can be noticed that the eggshell (Figure 4a) shows a rough surface with regular stripes. Remarkably, a series of randomly distributed pores (160 nm) is observed on the surface. This is mainly caused by (i) the decomposition of organic matter; and (ii) the exposure of natural open pores of the eggshell, which has also been reported in previous study [31]. Moreover, Figure 4b of the  $TiO_2$  sample display a typical granulated particles morphology. The hybridization of eggshell with  $TiO_2$  (Figure 4c) revealed that the surface of eggshell was covered with  $TiO_2$  nanoparticles, establishing an intimate interfacial contact between the  $TiO_2$  and eggshell components. The EDS analysis of the TE (Figure 4d) shows that Ca, Ti and O elements existed in the samples, indicating that  $TiO_2$ -eggshell compound material was successfully prepared. Additionally, the EDS element mapping analysis (Figure 4e,f) confirms the uniform distribution of Ti and Ca elements throughout the composite.

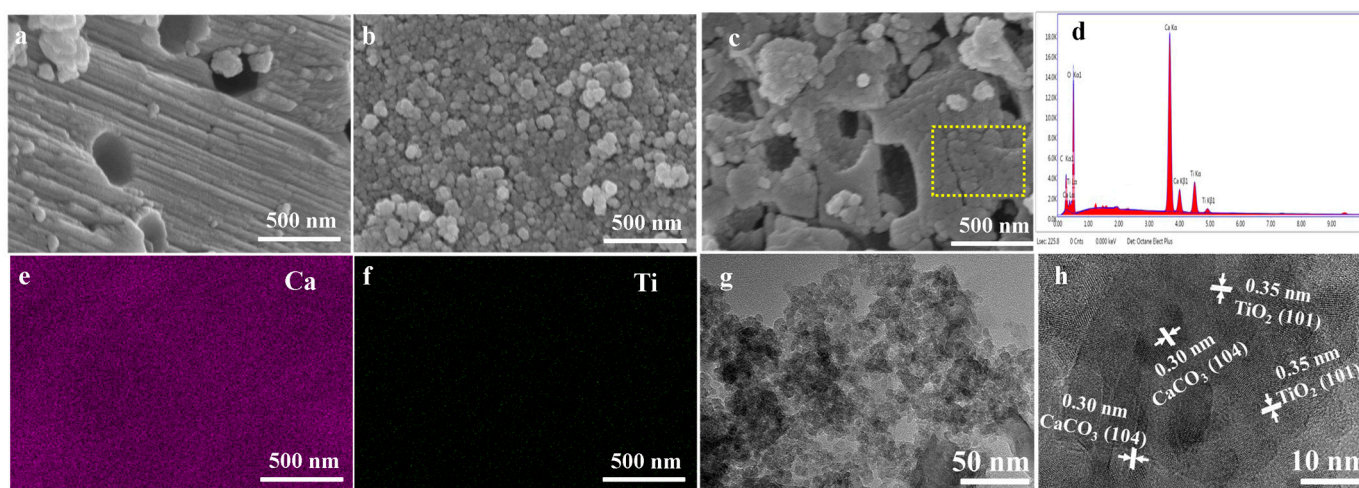


**Figure 4.** SEM images of (a) eggshell, (b)  $TiO_2$  and (c) TE; the EDS spectrum of (d) TE; the element mapping spectrum of a selected yellow rectangle is shown in (c), (e) Ca, (f) Ti; (g) TEM and (h) high resolution TEM (HRTEM) images of TE.

To obtain more detailed structural and micromorphology information of the TE composite, transmission electron microscopy (TEM) has been carried out. As shown in Figure 4g, the TEM image shows that  $TiO_2$  nanoparticles are evenly immobilized on the surface of eggshell. High resolution TEM analysis displays lattice fringes of 0.35 nm, corresponding to the (101) facet of anatase  $TiO_2$  [32]. Notably, the hybridization of  $TiO_2$  with eggshell had no obvious influence on the lattice structure of  $TiO_2$ , as shown in Figure 4h.

The photochemical activities of the as-obtained samples were evaluated by monitoring the maximal absorbance of TC at 357 nm via UV–vis spectrum under simulative solar light irradiation. Before light irradiation, the suspension was stirred for 3 h in dark to establish an

adsorption-desorption equilibrium (Figure 5a). Figure 5b shows that pure  $\text{TiO}_2$  displays an obvious photocatalytic activity in the system with 88.6% degradation efficiency of TC. As a typical photocatalyst, the degradation ability of  $\text{TiO}_2$  originated from the generation of ROS, such as  $\cdot\text{OH}$  and  $\text{h}^+$  under illumination [33]. Notably, the eggshell also displays obvious photoactivity (63.7%) under simulated solar light, which is markedly more active than the case in darkness. This is mainly attributed to the fact that the abundance of  $\text{CO}_3^{2-}/\text{HCO}_3^-$  in aqueous can be stimulated by the directly photolysis, which induces  $\cdot\text{CO}_3^-$  susceptible for degradation [24]. In comparison, the TE presents the highest degradation efficiency of 92.0%, which is higher than that of  $\text{TiO}_2$  and eggshell. Especially in the first ten minutes of the reaction, TE showed much higher photocatalytic activity than  $\text{TiO}_2$  and eggshell. The significantly improved efficiency can be ascribed to the fact that the carbonate radical ( $\cdot\text{CO}_3^-$ ) is a transient species with high selectivity, and it has a strong redox capacity for aromatic compounds containing phenol. In addition, the intimate hybridization of  $\text{TiO}_2$  and eggshell helps to accelerate the formation of  $\cdot\text{CO}_3^-$  [34,35]. Furthermore, the degradation efficiency of TC over TE drops slightly from 92.0% to 91.8% after five cycling tests, as shown in Figure 6a, which demonstrates that the  $\text{TiO}_2$ -eggshell composite has good stability of photocatalytic activity. XRD pattern of TE of before and after solar light irradiation (Figure 6b) shows that the intensities of characteristic XRD peaks of  $\text{TiO}_2$  were unchanged and that of the eggshell became lower, indicating that  $\text{CaCO}_3$  was consumed to produced  $\cdot\text{CO}_3^-$ .

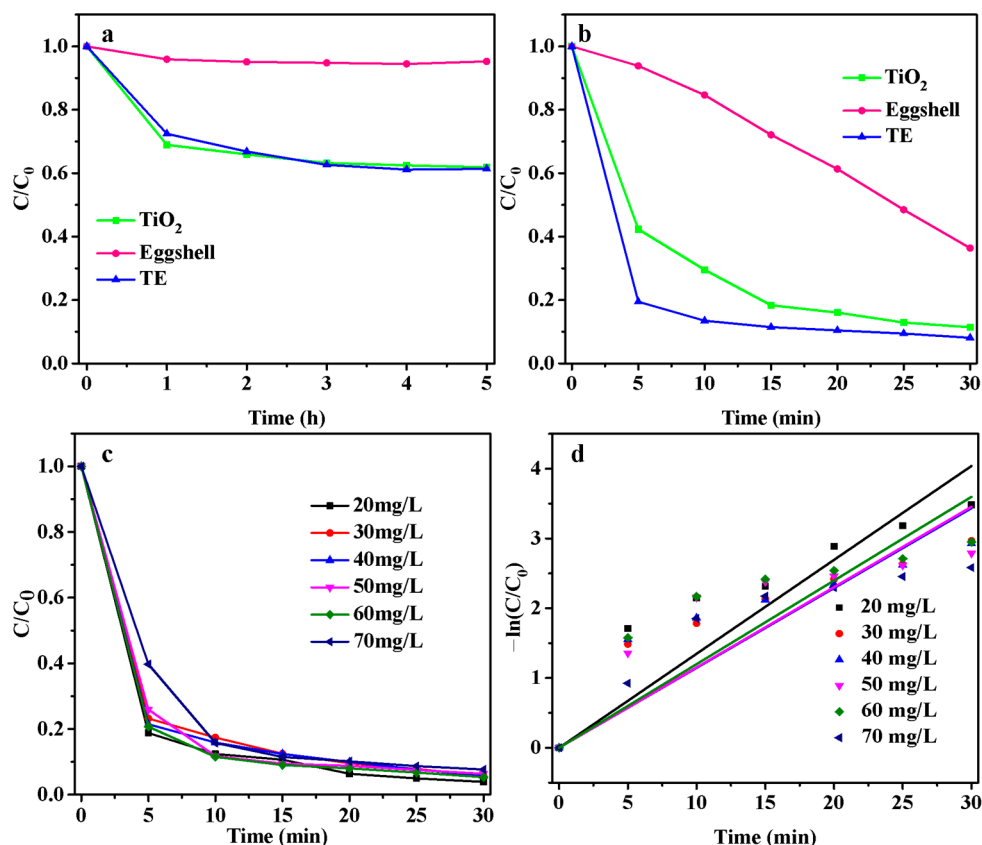


**Figure 5.** Degradation curves of tetracycline hydrochloride (TC) by the as-obtained samples (a) in dark conditions and (b) under simulated solar light illumination; the impact of initial TC concentrations (c) and kinetic curves of TC degradation (d).

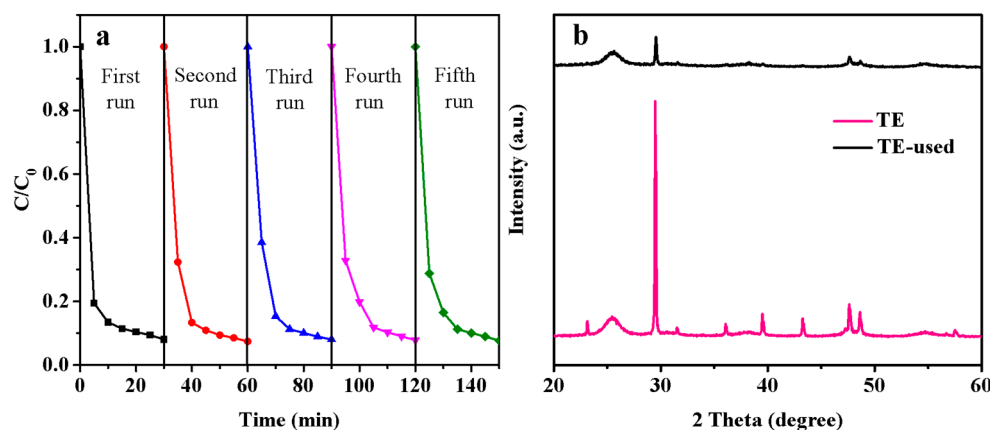


**Figure 6.** (a) Cycling curves of the TC over TE under solar light irradiation and (b) XRD pattern of TE of before and after solar light irradiation.

The kinetic data for the degradation of TC in the presence of eggshell, TiO<sub>2</sub> and TE fit well with the pseudo-first-order model, as shown in Equation (3) and Table 2 [36].

$$\ln\left(\frac{C_0}{C_t}\right) = kt \quad (3)$$

where  $C_0$  is the initial concentration of TC before irradiation,  $C_t$  is the concentration of TC at a certain interval of time ( $t$ ) under solar light irradiation and  $k$  is the apparent rate constant. As shown in Table 2, the  $k$  value of the TE composite ( $0.226 \text{ min}^{-1}$ ) was almost 10 times higher than that of eggshell ( $0.0216 \text{ min}^{-1}$ ) and double that of TiO<sub>2</sub> ( $0.107 \text{ min}^{-1}$ ). In addition, the impact of initial TC concentration toward the photocatalytic elimination efficiency over TE was also discussed. As shown in Figure 5c, the degradation efficiency declined mildly from 96.1% to 91.3% when the initial TC concentration increased from 20 to 70 mg/L, respectively. Besides, Figure 4 exhibited that the reaction also follows a pseudo-first order kinetic model, and the  $k$  values were similar ranged from  $0.1057$  to  $0.1347 \text{ min}^{-1}$ . Therefore, it can be deduced that the initial TC concentration had negligible influence on the photocatalytic reaction.

**Table 2.** Kinetics parameters of the pseudo-first-order model for TC degradation by the as-prepared samples.

Samples	Degradation (%)	$k$ ( $\text{min}^{-1}$ )	$R^2$
Eggshell	63.7	0.0216	0.993
TiO <sub>2</sub>	88.6	0.107	0.979
TE	92.0	0.226	0.999

The intermediates generated during the TC degradation was measured by FT-IR spectra. As shown in Figure 7, before the photodegradation with TE, the broad peaks centered at  $3364$  and  $3307 \text{ cm}^{-1}$  were attributed to NH<sub>2</sub> symmetric stretching vibrations and O–H stretching vibrations on TC. The absorption peak at  $3099 \text{ cm}^{-1}$  was associated with C–H stretching vibration of aromatic hydrocarbon. Together, the peaks at  $2963$  and  $2930 \text{ cm}^{-1}$  were respectively assigned to C–H(CH<sub>3</sub>) and C–H(CH<sub>2</sub>) antisymmetric stretching vibrations. The peaks at  $1671$  and  $1228 \text{ cm}^{-1}$  were linked to the carbonyl group and C–OH stretching vibration, respectively, while peaks at  $1616 \text{ cm}^{-1}$  could be inferred to the carbonyl group in the hexatomic ring. Furthermore, the  $1582$ ,  $1456$  and  $1382 \text{ cm}^{-1}$  bands constitute the skeleton vibration of the aromatic –C=C–.



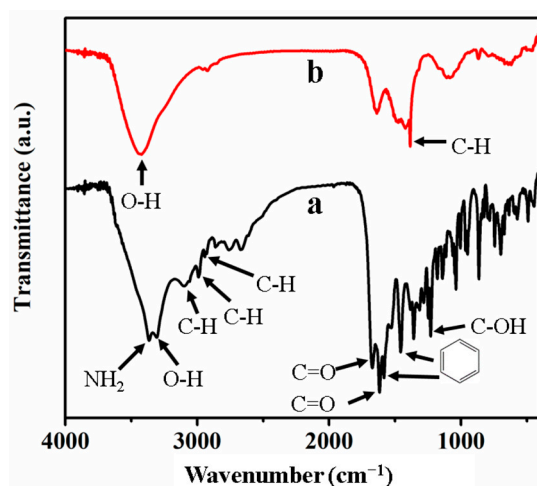


**Figure 7.** FT-IR spectra of TC (a) before and (b) after 30 min photodegradation.

In contrast, after light irradiation, the spectrum (Figure 7) of the degraded TC became smooth, indicating that the functional groups of tetracycline were decomposed or removed. The peaks at 3364 and 3307  $\text{cm}^{-1}$  disappeared. Meanwhile, a broad peak that assigned to hydroxyl stretching vibrations in moisture appeared at 3423  $\text{cm}^{-1}$ , suggesting that the amine and hydroxyl group in phenol was eliminated. Moreover, the flexural vibrational peak of C-H at 1384  $\text{cm}^{-1}$  was apparently weakened. Additionally, the peaks at 1616, 1582 and 1456  $\text{cm}^{-1}$  completely disappeared after the reaction, denoting the removal of carbonyl group and aromatic  $-\text{C}=\text{C}-$ .

To further investigate the intermediates generated in the system, LC-QTOF-MS was undertaken, as shown in Figure 8. It is obvious that the intensity of different products was weakened and even disappeared in 30 min. A possible degradation pathway of TC was proposed in Scheme 1. Compared to parent TC,  $M_1$  ( $m/z$  447) may be generated from TC via a hydroxylation process occurring on the carbonyl, which is consistent with a recent study [37]. Besides,  $M_2$  ( $m/z$  474) was generated from TC via hydroxylation and subsequently subjected to attack by reactive radicals, which has been documented in Yang et al.'s study [38]. Similarly,  $M_3$  ( $m/z$  432) was identified and arose from the hydroxylation and the removal of two N-methyl groups, respectively, which further led to the generation of  $M_4$  ( $m/z$  402) through detachment of two amino groups. This is due to the weak bond energy of N-C [39]. Additionally, the generation of  $M_5$  ( $m/z$  430) and  $M_6$  ( $m/z$  416) were attributed to successive N-dealkylation steps of TC. On one hand, after the reaction of dehydroxylation, the C-C double bond of  $M_6$  was attacked by the reactive species in the system, and finally, the intermediate product degrades to  $M_7$  ( $m/z$  349) through intramolecular condensation, which has been described in a previous research [37]. On the other hand, the  $M_6$  can be further fragmented into  $M_8$  ( $m/z$  316) via dehydroxylation, deamination, opening of the hexatomic ring, deethylation and additive reaction. Then the  $M_8$  is transformed into  $M_9$  ( $m/z$  272) via deacetylation. A similar degradation pathway has been suggested in the recent research of Yang et al [38].

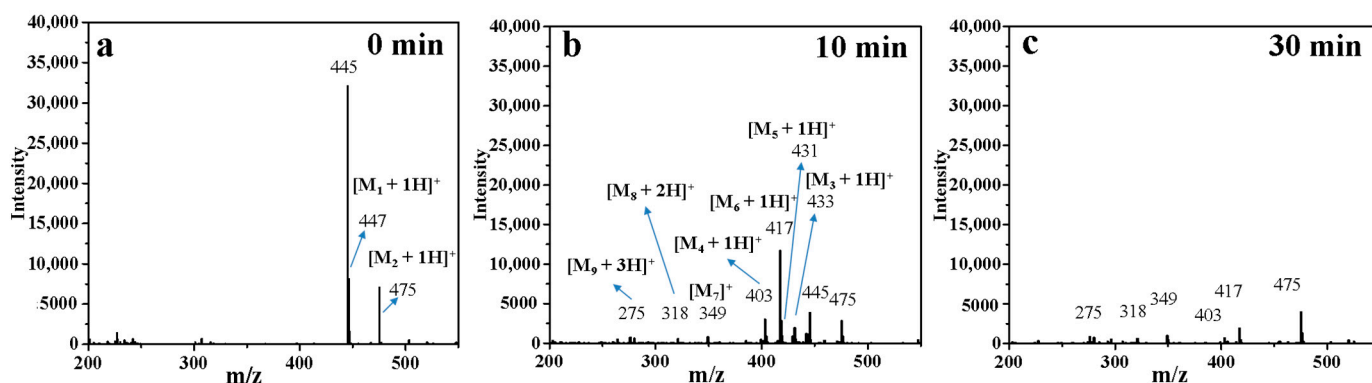
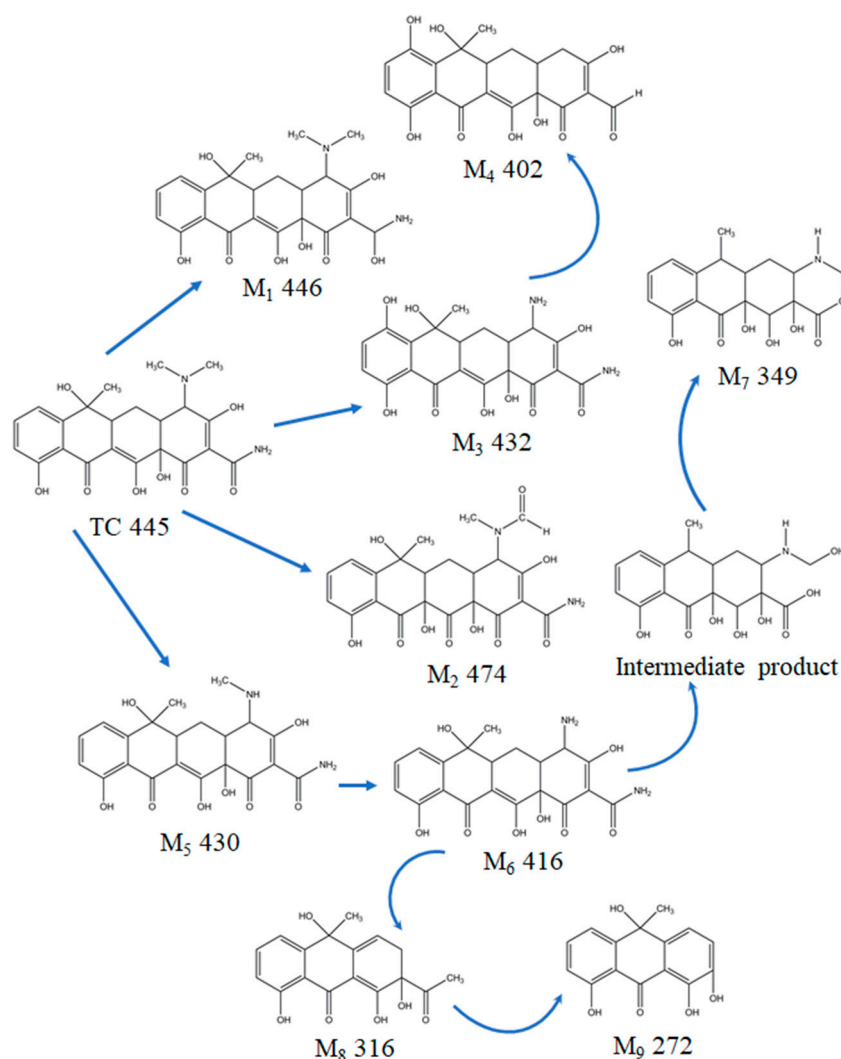


**Figure 8.** LC-QTOF-MS mass spectra of transformation by products during the photodegradation of TE at different reaction times.



**Scheme 1.** Suggested photodegradation pathway of TC.

Identifying the main reactive radicals is important to reveal the mechanism of the TC degradation over the TE composite. Different radical scavengers of AO (a quencher of  $h^+$ ), BQ (a quencher of  $\cdot O_2^-$ ), IPA (a quencher of  $\cdot OH$ ) and 4-CP (a quencher of  $\cdot CO_3^-$ ) have been added into TC aqueous solution, respectively [18,40]. As shown in Figure 9, the photoactivity of  $TiO_2$  shows a dramatic reduction from 88.6% to 38.4%, and to 49.6% after the addition of BQ and AO, respectively (Figure 9a), implying that  $\cdot O_2^-$  and  $h^+$  play

dominant roles in the degradation of TC when using TiO<sub>2</sub>. However, fuzzy reduction is observed after adding IPA, which suggests that the ·OH radical plays a minor role in the process.

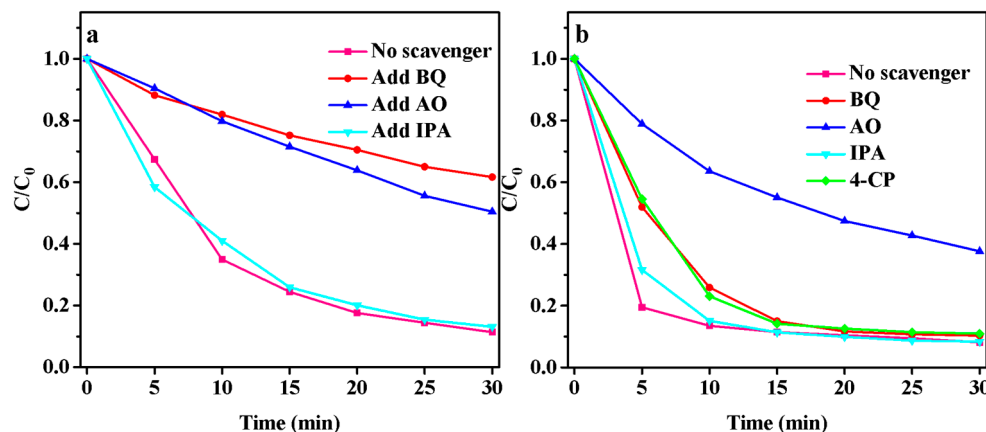


**Figure 9.** Active species trapping experiment on TC degradation in the presence of (a) TiO<sub>2</sub> and (b) TE.

In comparison, the TE displays a different mechanism for the degradation of TC. As depicted in Figure 9b, when BQ and AO were added, the photodegradation efficiency of TC declined from 92.0% to 89.8% and 62.4%, respectively. Moreover, the degradation efficiency was also clearly worse than after adding IPA, which indicates that the ·OH was also involved in the photoreaction process, from the result it could be claimed that the consumption of ·CO<sub>3</sub><sup>−</sup> could promote the generation of ·OH to some extent. Furthermore, when using the TE composite directly, the 4-CP capturer inhibited the degradation activity of TC obviously, which implied that the ·CO<sub>3</sub><sup>−</sup> radical also plays an important role in this photocatalytic system. These results were consistent with the previous photodegradation research that involves the ·CO<sub>3</sub><sup>−</sup> species [18]. Therefore, the generation of ·CO<sub>3</sub><sup>−</sup> radical and the synergistic effect of ·CO<sub>3</sub><sup>−</sup>, h<sup>+</sup>, ·O<sub>2</sub><sup>−</sup> and ·OH contribute to the significantly improved degradation efficiency.

Results of the statistical analysis are detailed in Table 3. An empirical relationship between response and variables was found. The result was in good accordance with the experiment data, for which the TC degradation efficiencies ranged from 24.6 to 96.9%. The most appropriate method to arrive at a final model via regression analysis in this photochemical degradation system can be ascribed to Equation (4):

$$Y = -0.851 + 0.025 \times A + 2.840 \times B + 0.362 \times C - 0.012 \times D - 0.106 \times AB + 1.04E - 03 \times AC + 1.99E - 04 \times AD + 0.039 \times BC + 0.087 \times BD + 5.03E - 04 \times CD - 5.42E - 04 \times A^2 - 26.055 \times B^2 - 0.023 \times C^2 - 4.72E - 05 \times D^2 \quad (4)$$

where Y is the efficiency of TC degradation, A is irradiation time, B is catalyst dosage, C is pH and D is initial concentration. Additionally, analysis of variance (ANOVA) for the quadratic polynomial regression equation of predicted values is also depicted in Table 3. All parameters in this model are ascertained via ANOVA (Table 4). The F value (9.7) and p values (<0.0001) suggest that the model could well explain the relationships between TC degradation efficiency and the four system parameters mentioned above. Furthermore, the F values of A ( $p < 0.0001$ ), AB ( $p = 0.0233$ ), BD ( $p = 0.0005$ ), A<sup>2</sup> ( $p = 0.0114$ ), B<sup>2</sup> ( $p = 0.0004$ ) and C<sup>2</sup> ( $p = 0.0014$ ) were also statistically significant model terms. The good correlation between the experimental and standard estimations ( $R^2 = 0.906$ ) means that the selected factors (irradiation time, dosage, pH and concentration) and regression model exhibited a good prediction of TC degradation efficiency in aqueous solution. Pursuant to this model, the effect of respective factors on the photodegradation of TC by TE was proceeded as follows: dosage > irradiation time > pH > concentration. Here the optimal photodegradation

condition was stated: irradiation time of 27 min, catalyst dosage of 0.15 g, pH of 8.4 and initial concentration of 78 mg/L, yielding a high degradation rate for TC of 99.9%. It can also be asserted that the interaction between catalyst dosage and irradiation time had the largest effect on the photodegradation of TC by TE.

The contour nature of Figure 10 shows the relationships in terms of operating parameters, which comprises irradiation time, catalyst dosage, pH, TC concentration and their effect on TC degradation efficiency at room temperature (25 °C). As shown in Figure 10a, insufficient TE dosage and low irradiation time does not encourage TC degradation. The photodegradation rate of TC increases comparably when the pH < 8.5 but fell away considerably when the pH > 8.5 regardless of irradiation time (Figure 10b). A large amount of TC is decomposed when the irradiation time increased with the indicated concentrations ranges from 20 to 80 mg/L (Figure 10c). The photodegradation rate of TC apparently improved when the pH < 8.5, yet this was inhibited considerably when the pH > 8.5, this refers to the change in catalyst dosage from 0.02 to 0.18 g (Figure 10d). It is notable that degradation efficiency increased when the catalyst dosage < 0.1 g but declined significantly when the catalyst dosage > 0.1 g, when the concentrations were increased (Figure 10e). Better degradation efficiency of TC was obtained at pH < 8.5 with the initial concentration ranging from 20 to 80 mg/L. However, degradation efficiency declined when the pH was above 8.5 (Figure 10f). Collectively, the results demonstrate that each two different variables had quite different effects on the degradation rate of TC, and the interaction among the selected process parameters were confirmed.

**Table 3.** Response center combination test design and results.

Run	A	B	C	D	TC Degradation Efficiency (%)	
					Observed	Predicted
1	16	0.1	6	20	73.0	77.1
2	30	0.1	8.5	80	91.6	108.4
3	2	0.1	8.5	20	63.5	67.4
4	30	0.1	11	50	89.9	99.4
5	2	0.02	8.5	50	27.0	28.1
6	16	0.1	8.5	50	89.9	94.4
7	16	0.1	11	80	87.3	82.0
8	30	0.1	8.5	20	96.9	95.0
9	30	0.18	8.5	50	85.0	82.3
10	16	0.1	8.5	50	89.8	94.4
11	16	0.02	8.5	20	92.2	91.1
12	16	0.1	8.5	50	89.7	94.4
13	16	0.1	8.5	50	89.8	94.4
14	2	0.1	11	50	44.3	47.7
15	16	0.02	6	50	42.8	55.0
16	30	0.02	8.5	50	92.0	96.2
17	30	0.1	6	50	78.1	83.8
18	16	0.1	8.5	50	89.7	94.4
19	2	0.18	8.5	50	67.3	61.7
20	16	0.1	6	80	74.7	66.1
21	16	0.18	8.5	20	51.5	59.2
22	16	0.18	11	50	64.4	73.2
23	16	0.02	8.5	80	45.0	46.0
24	2	0.1	6	50	47.2	46.7
25	2	0.1	8.5	80	24.7	47.3
26	16	0.18	6	50	52.9	63.3
27	16	0.1	11	20	70.5	77.9
28	16	0.02	11	50	51.3	61.8
29	16	0.18	8.5	80	87.6	97.6

**Table 4.** The response surface quadratic model via ANOVA for the photodegradation of TC.

Source	Sum of Squares	DF	Mean Square	F Value	<i>p</i> -Value Prob > F	
Model	1.17	14	0.084	9.7	<0.0001	significant
A	0.56	1	0.56	65.02	<0.0001	
B	0.029	1	0.029	3.31	0.0902	
C	0.013	1	0.013	1.47	0.2459	
D	0.011	1	0.011	1.29	0.2751	
AB	0.056	1	0.056	6.48	0.0233	
AC	$5.32 \times 10^{-3}$	1	$5.32 \times 10^{-3}$	0.62	0.4458	
AD	0.028	1	0.028	3.24	0.0936	
BC	$2.42 \times 10^{-4}$	1	$2.42 \times 10^{-4}$	0.028	0.8696	
BD	0.17	1	0.17	20.1	0.0005	
CD	$5.70 \times 10^{-3}$	1	$5.70 \times 10^{-3}$	0.66	0.4303	
A <sup>2</sup>	0.073	1	0.073	8.47	0.0114	
B <sup>2</sup>	0.18	1	0.18	20.88	0.0004	
C <sup>2</sup>	0.14	1	0.14	15.78	0.0014	
D <sup>2</sup>	0.012	1	0.012	1.36	0.2635	
Residual	0.12	14	$8.64 \times 10^{-3}$			
Lack of Fit	0.12	10	0.012			
Pure Error	0	4	0			
Cor Total	1.29	28				
R <sup>2</sup>			0.906			

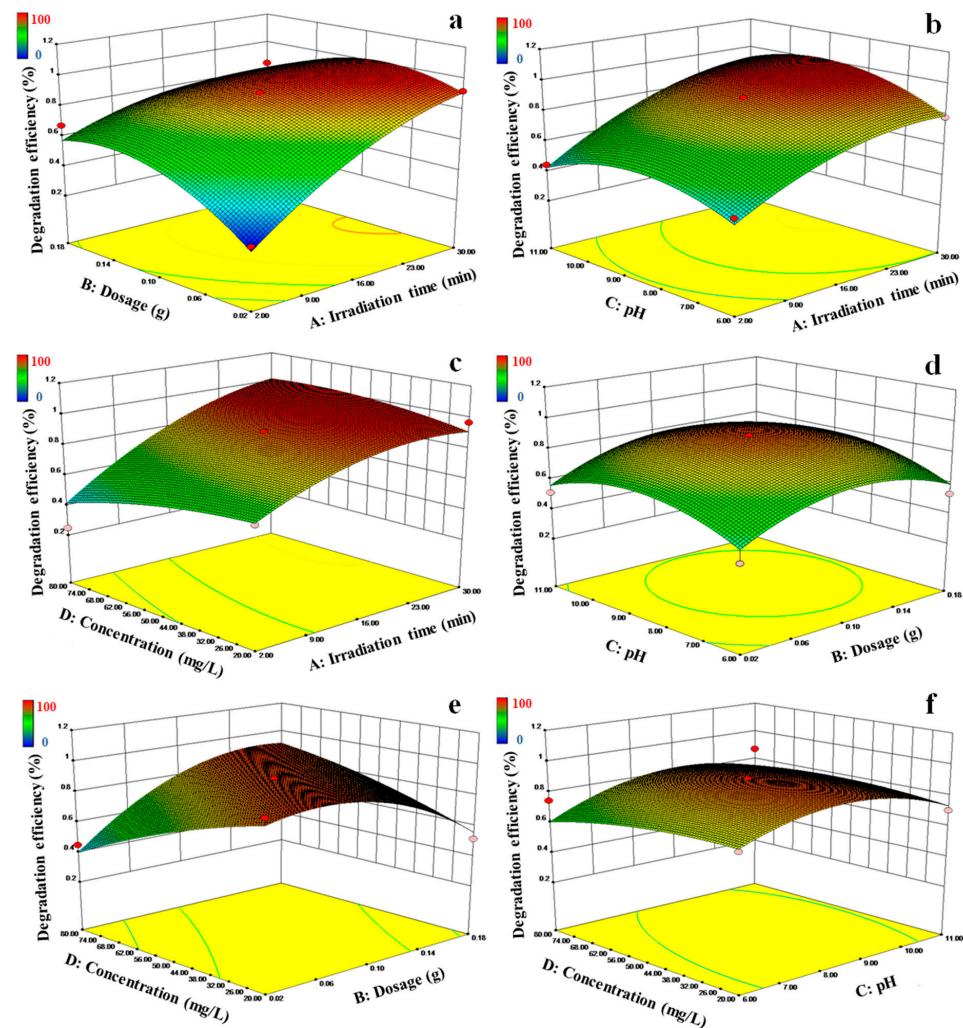


**Figure 10.** Response surfaces for TC degradation: (a) irradiation time–dosage, (b) irradiation time–pH, (c) irradiation time–concentration, (d) dosage–pH, (e) dosage–concentration and (f) pH–concentration.



#### 4. Conclusions

In this research, a novel TiO<sub>2</sub>-eggshell (TE) material was successfully fabricated as an efficient catalyst for the targeted degradation of tetracycline hydrochloride (TC) under solar light irradiation. A possible photodegradation pathway of TC was proposed, which suffered deamination, dehydroxylation or removal of other functional groups. The observed high efficiency of TE was mainly ascribed to the in-situ formation of carbonate radical ( $\cdot\text{CO}_3^-$ ) and the synergistic effect of  $\cdot\text{CO}_3^-$ ,  $\text{h}^+$ ,  $\cdot\text{O}_2^-$  and  $\cdot\text{OH}$ . The best degradation condition for TC was at an initial concentration of 78 mg/L, pH of 8.4, TE dosage of 0.15 g and irradiated by simulated solar light for 27 min. The corresponding degradation ratio reached 99.9%. The present work shows that the simple yet effective TE composite had great potential for targeted remediating antibiotics from wastewaters under solar light illumination.

**Author Contributions:** Z.H. and J.W. performed the research, analyzed the data and wrote the paper; Z.H., M.-Q.Y., Q.Q., and X.-P.L. revised the paper. L.X. and H.X. were the supervisor and revised the paper. All authors have read and agreed to the published version of the manuscript.

**Funding:** This work was supported financially by the National Natural Science Foundation of China (NSFC 21875037 and 51502036), National Key Research and Development Program of China (2016YFB0302303 and 2019YFC1908203).

**Institutional Review Board Statement:** Not applicable.

**Informed Consent Statement:** Not applicable.

**Data Availability Statement:** All data is contained within the article.

**Conflicts of Interest:** The authors declare that they have no conflict of interest.

#### References

1. Wang, C.; Wu, Y.L.; Lu, J.; Zhao, J.; Cui, J.Y.; Wu, X.L.; Yan, Y.S.; Huo, P.W. Bioinspired Synthesis of Photocatalytic Nanocomposite Membranes Based on Synergy of Au-TiO<sub>2</sub> and Polydopamine for Degradation of Tetracycline under Visible Light. *ACS Appl. Mater. Interfaces* **2017**, *9*, 23687–23697. [[CrossRef](#)]
2. Tran, N.H.; Reinhard, M.; Gin, K.Y. Occurrence and fate of emerging contaminants in municipal wastewater treatment plants from different geographical regions—a review. *Water Res.* **2018**, *133*, 182–207. [[CrossRef](#)]
3. Michael, I.; Rizzo, L.; Mc Ardell, C.S.; Manaia, C.M.; Merlin, C.; Schwartz, T.; Dagot, C.; Fatta-Kassinos, D. Urban wastewater treatment plants as hotspots for the release of antibiotics in the environment: A review. *Water Res.* **2013**, *47*, 957–995. [[CrossRef](#)] [[PubMed](#)]
4. Qi, N.; Wang, P.F.; Wang, C.; Ao, Y.H. Effect of a typical antibiotic (tetracycline) on the aggregation of TiO<sub>2</sub> nanoparticles in an aquatic environment. *J. Hazard. Mater.* **2018**, *341*, 187–197. [[CrossRef](#)]
5. Liu, X.H.; Lu, S.Y.; Guo, W.; Xi, B.D.; Wang, W.L. Antibiotics in the aquatic environments: A review of lakes, China. *Sci. Total Environ.* **2018**, *627*, 1195–1208. [[CrossRef](#)] [[PubMed](#)]
6. Le-Minh, N.; Khan, S.J.; Drewes, J.E.; Stuetz, R.M. Fate of antibiotics during municipal water recycling treatment processes. *Water Res.* **2010**, *44*, 4295–4323. [[CrossRef](#)] [[PubMed](#)]
7. Yang, Y.Y.; Song, W.J.; Lin, H.; Wang, W.B.; Du, L.N.; Xing, W. Antibiotics and antibiotic resistance genes in global lakes: A review and meta-analysis. *Environ. Int.* **2018**, *116*, 60–73. [[CrossRef](#)]
8. Reddy, P.A.; Reddy, P.V.; Kwon, E.; Kim, K.H.; Akter, T.; Kalagara, S. Recent advances in photocatalytic treatment of pollutants in aqueous media. *Environ. Int.* **2016**, *91*, 94–103. [[CrossRef](#)]
9. Xing, Z.P.; Zhang, J.Q.; Cui, J.Y.; Yin, J.W.; Zhao, T.Y.; Kuang, J.Y.; Xiu, Z.Y.; Wan, N.; Zhou, W. Recent advances in floating TiO<sub>2</sub>-based photocatalysts for environmental application. *Appl. Catal. B* **2018**, *225*, 452–467. [[CrossRef](#)]
10. Xiao, T.T.; Tang, Z.; Yang, Y.; Tang, L.Q.; Zhou, Y.; Zou, Z.G. In situ construction of hierarchical WO<sub>3</sub>/g-C<sub>3</sub>N<sub>4</sub> composite hollow microspheres as a Z-scheme photocatalyst for the degradation of antibiotics. *Appl. Catal. B* **2018**, *220*, 417–428. [[CrossRef](#)]
11. Jiang, L.B.; Yuan, X.Z.; Zeng, G.M.; Chen, X.H.; Wu, Z.B.; Liang, J.; Zhang, J.; Wang, H.; Wang, H. Phosphorus- and Sulfur-Codoped g-C<sub>3</sub>N<sub>4</sub>: Facile Preparation, Mechanism Insight, and Application as Efficient Photocatalyst for Tetracycline and Methyl Orange Degradation under Visible Light Irradiation. *ACS Sustain. Chem. Eng.* **2017**, *5*, 5831–5841. [[CrossRef](#)]
12. He, X.; Fang, H.; Gosztola, D.J.; Jiang, Z.; Jena, P.; Wang, W.N. Mechanistic Insight into Photocatalytic Pathways of MIL-100(Fe)/TiO<sub>2</sub> Composites. *ACS Appl. Mater. Interfaces* **2019**, *11*, 12516–12524. [[CrossRef](#)]
13. Schneider, J.; Matsuoka, M.; Takeuchi, M.; Zhang, J.L.; Horiuchi, Y.; Anpo, M.; Bahnemann, D.W. Understanding TiO<sub>2</sub> photocatalysis: Mechanisms and materials. *Chem. Rev.* **2014**, *114*, 9919–9986. [[CrossRef](#)]

14. Shi, H.M.; Ni, J.; Zheng, T.L.; Wang, X.N.; Wu, C.F.; Wang, Q.H. Remediation of wastewater contaminated by antibiotics. A review. *Environ. Chem. Lett.* **2019**, *18*, 345–360. [[CrossRef](#)]
15. Isari, A.A.; Mehregan, M.; Mehregan, S.; Hayati, F.; Rezaei Kalantary, R.; Kakavandi, B. Sono-photocatalytic degradation of tetracycline and pharmaceutical wastewater using WO<sub>3</sub>/CNT heterojunction nanocomposite under US and visible light irradiations: A novel hybrid system. *J. Hazard. Mater.* **2020**, *390*, 122050. [[CrossRef](#)] [[PubMed](#)]
16. Canonica, S.; Kohn, T.; Mac, M.; Real, F.J.; Wirz, J.; von Gunten, U. Photosensitizer Method to Determine Rate Constants for the Reaction of Carbonate Radical with Organic Compounds. *Environ. Sci. Technol.* **2005**, *39*, 9182–9188. [[CrossRef](#)]
17. Yadav, T.; Mungray, A.A.; Mungray, A.K. Generation of TiO<sub>2</sub> nanoparticle-based acacia saturated eggshell bio-composite for pathogen removal. *Environ. Nanotechnol. Monit. Manag.* **2017**, *9*, 50–57.
18. Liu, Y.Q.; He, X.X.; Duan, X.D.; Fu, Y.S.; Dionysiou, D.D. Photochemical degradation of oxytetracycline: Influence of pH and role of carbonate radical. *Chem. Eng. J.* **2015**, *276*, 113–121. [[CrossRef](#)]
19. Burns, J.M.; Cooper, W.J.; Ferry, J.L.; King, D.W.; Di Mento, B.P.; McNeill, K.; Miller, C.J.; Miller, W.L.; Peake, B.M.; Rusak, S.A.; et al. Methods for reactive oxygen species (ROS) detection in aqueous environments. *Aquat. Sci.* **2012**, *74*, 683–734. [[CrossRef](#)]
20. Wang, H.M.; You, C.F.; Tan, Z.C. Enhanced photocatalytic oxidation of SO<sub>2</sub> on TiO<sub>2</sub> surface by Na<sub>2</sub>CO<sub>3</sub> modification. *Chem. Eng. J.* **2018**, *350*, 89–99. [[CrossRef](#)]
21. Buxton, G.V.; Greenstock, C.L.; Helman, W.P.; Ross, A.B. Critical Review of rate constants for reactions of hydrated electrons, hydrogen atoms and hydroxyl radicals (·OH/O<sup>-</sup> in Aqueous Solution. *J. Phys. Chem. Ref. Data* **1988**, *17*, 513–886. [[CrossRef](#)]
22. Zhu, C.Z.; Wang, Y.T.; Jiang, Z.F.; Liu, A.N.; Pu, Y.; Xian, Q.M.; Zou, W.X.; Sun, C. Ultrafine Bi<sub>3</sub>TaO<sub>7</sub> Nanodot-Decorated V, N Codoped TiO<sub>2</sub> Nanoblocks for Visible-Light Photocatalytic Activity: Interfacial Effect and Mechanism Insight. *ACS Appl. Mater. Interfaces* **2019**, *11*, 13011–13021. [[CrossRef](#)]
23. Wang, J.; Sun, S.J.; Pan, L.; Xu, Z.Q.; Ding, H.; Li, W. Preparation and Properties of CaCO<sub>3</sub>-Supported Nano-TiO<sub>2</sub> Composite with Improved Photocatalytic Performance. *Materials* **2019**, *12*, 3369. [[CrossRef](#)] [[PubMed](#)]
24. Wang, J.Q.; Qian, Q.R.; Chen, Q.; Liu, X.P.; Luo, Y.; Xue, H.; Li, Z. Significant role of carbonate radicals in tetracycline hydrochloride degradation based on solar light-driven TiO<sub>2</sub>-seashell composites: Removal and transformation pathways. *Chin. J. Catal.* **2020**, *41*, 1511–1521. [[CrossRef](#)]
25. Chen, X.; Li, C.W.; Wang, J.; Li, J.; Luan, X.; Li, Y.; Xu, R.; Wang, B. Investigation on solar photocatalytic activity of TiO<sub>2</sub> loaded composite: TiO<sub>2</sub>/Eggshell, TiO<sub>2</sub>/Clamshell and TiO<sub>2</sub>/CaCO<sub>3</sub>. *Mater. Lett.* **2010**, *64*, 1437–1440. [[CrossRef](#)]
26. Ding, Q.; Kang, Z.; Cao, L.; Lin, M.; Lin, H.; Yang, D.-P. Conversion of waste eggshell into difunctional Au/CaCO<sub>3</sub> nanocomposite for 4-Nitrophenol electrochemical detection and catalytic reduction. *Appl. Surf. Sci.* **2020**, *510*, 145526. [[CrossRef](#)]
27. Fu, X.Z.; Zeltner, W.A.; Yang, Q.; Anderson, M.A. Catalytic Hydrolysis of Dichlorodifluoromethane (CFC-12) on Sol-Gel-Derived Titania Unmodified and Modified with H<sub>2</sub>SO<sub>4</sub>. *J. Catal.* **1997**, *168*, 482–490. [[CrossRef](#)]
28. Li, B.; Gan, L.; Owens, G.; Chen, Z. New nano-biomaterials for the removal of malachite green from aqueous solution via a response surface methodology. *Water Res.* **2018**, *146*, 55–66. [[CrossRef](#)] [[PubMed](#)]
29. Gupta, V.K.; Agarwal, S.; Asif, M.; Fakhri, A.; Sadeghi, N. Application of response surface methodology to optimize the adsorption performance of a magnetic graphene oxide nanocomposite adsorbent for removal of methadone from the environment. *J. Colloid Interface Sci.* **2017**, *497*, 193–200. [[CrossRef](#)]
30. Sun, H.; He, Q.R.; She, P.; Zeng, S.; Xu, K.L.; Li, J.Y.; Liang, S.; Liu, Z.N. One-pot synthesis of Au@TiO<sub>2</sub> yolk-shell nanoparticles with enhanced photocatalytic activity under visible light. *J. Colloid Interface Sci.* **2017**, *505*, 884–891. [[CrossRef](#)]
31. Cree, D.; Rutter, A. Sustainable Bio-Inspired Limestone Eggshell Powder for Potential Industrialized Applications. *ACS Sustain. Chem. Eng.* **2015**, *3*, 941–949. [[CrossRef](#)]
32. Li, Y.H.; Lv, K.L.; Ho, W.K.; Dong, F.; Wu, X.; Xia, Y. Hybridization of rutile TiO<sub>2</sub> (rTiO<sub>2</sub>) with g-C<sub>3</sub>N<sub>4</sub> quantum dots (CN QDs): An efficient visible-light-driven Z-scheme hybridized photocatalyst. *Appl. Catal. B* **2017**, *202*, 611–619. [[CrossRef](#)]
33. Moreira, N.F.F.; Narciso-da-Rocha, C.; Polo-Lopez, M.I.; Pastrana-Martinez, L.M.; Faria, J.L.; Manaia, C.M.; Fernandez-Ibanez, P.; Nunes, O.C.; Silva, A.M.T. Solar treatment (H<sub>2</sub>O<sub>2</sub>, TiO<sub>2</sub>-P25 and GO-TiO<sub>2</sub> photocatalysis, photo-Fenton) of organic micropollutants, human pathogen indicators, antibiotic resistant bacteria and related genes in urban wastewater. *Water Res.* **2018**, *135*, 195–206. [[CrossRef](#)] [[PubMed](#)]
34. Pelaez, M.; de la Cruz, A.A.; O’Shea, K.; Falaras, P.; Dionysiou, D.D. Effects of water parameters on the degradation of microcystin-LR under visible light-activated TiO<sub>2</sub> photocatalyst. *Water Res.* **2011**, *45*, 3787–3796. [[CrossRef](#)] [[PubMed](#)]
35. Zhang, G.; He, X.; Nadagouda, M.N.; O’Shea, K.E.; Dionysiou, D.D. The effect of basic pH and carbonate ion on the mechanism of photocatalytic destruction of cylindrospermopsin. *Water Res.* **2015**, *73*, 353–361. [[CrossRef](#)]
36. Al-Ekabi, H.; Serpone, N. Kinetics studies in heterogeneous photocatalysis. I. Photocatalytic degradation of chlorinated phenols in aerated aqueous solutions over titania supported on a glass matrix. *J. Phys. Chem.* **1988**, *92*, 5726–5731. [[CrossRef](#)]
37. Chen, Y.Y.; Ma, Y.L.; Yang, J.; Wang, L.Q.; Lv, J.M.; Ren, C.J. Aqueous tetracycline degradation by H<sub>2</sub>O<sub>2</sub> alone: Removal and transformation pathway. *Chem. Eng. J.* **2017**, *307*, 15–23. [[CrossRef](#)]
38. Yang, Y.; Zeng, Z.T.; Zhang, C.; Huang, D.L.; Zeng, G.M.; Xiao, R.; Lai, C.; Zhou, C.Y.; Guo, H.; Xue, W.J.; et al. Construction of iodine vacancy-rich BiOI/Ag@AgI Z-scheme heterojunction photocatalysts for visible-light-driven tetracycline degradation: Transformation pathways and mechanism insight. *Chem. Eng. J.* **2018**, *349*, 808–821. [[CrossRef](#)]

- 
39. Delépée, R.; Maume, D.; Le Bizec, B.; Pouliquen, H. Preliminary assays to elucidate the structure of oxytetracycline's degradation products in sediments: Determination of natural tetracyclines by high-performance liquid chromatography–fast atom bombardment mass spectrometry. *J. Chromatogr. B Biomed. Sci. Appl.* **2000**, *748*, 369–381. [[CrossRef](#)]
  40. Chen, Y.; Liu, K.R. Preparation and characterization of nitrogen-doped TiO<sub>2</sub>/diatomite integrated photocatalytic pellet for the adsorption-degradation of tetracycline hydrochloride using visible light. *Chem. Eng. J.* **2016**, *302*, 682–696. [[CrossRef](#)]